

1 A single-nucleus RNA sequencing atlas of the 2 postnatal retina of the shark *Scyliorhinus canicula*

3 Authors

6 Nicolás Vidal-Vázquez^{1,2,*}, Ismael Hernández-Núñez^{1,*}, Pablo Carballo-Pacoret^{1,3}, Sarah
7 Salisbury³, Paula R. Villamayor^{3,4}, Francisca Hervas-Sotomayor^{5,6}, Xuefei Yuan⁵, Francesco
8 Lamanna⁵, Céline Schneider⁵, Julia Schmidt⁵, Sylvie Mazan⁷, Henrik Kaessmann⁵, Fátima Adrio¹,
9 Diego Robledo^{3,8}, Antón Barreiro-Iglesias^{1,2}, Eva Candal^{1,2}

10 Affiliations

12 1. Departamento de Bioloxía Funcional, Facultade de Bioloxía, Universidade de Santiago de
13 Compostela, 15782, Santiago de Compostela, Spain

14 2. Aquatic One Health Research Center (ARCUS), Universidade de Santiago de Compostela,
15 15782, Santiago de Compostela, Spain

16 3. The Roslin Institute and Royal (Dick) School of Veterinary Studies, University of Edinburgh,
17 Edinburgh EH25 9RG, UK

18 4. Departamento de Zooloxía, Xenética e Antropoloxía Física, Facultade de Veterinaria,
19 Universidade de Santiago de Compostela, 27002, Lugo, Spain

20 5. Center for Molecular Biology (ZMBH), DKFZ-ZMBH Alliance, Heidelberg University,
21 Heidelberg, Germany

22 6. Current affiliation: INRAE, LPGP, Rennes, France

23 7. CNRS, Sorbonne Université, Biologie Intégrative des Organismes Marins, UMR7232-BIOM,
24 Banyuls-sur-Mer, France

25 8. Departamento de Zooloxía, Xenética e Antropoloxía Física, Facultade de Bioloxía,
26 Universidade de Santiago de Compostela, 15782, Santiago de Compostela, Spain

27 * These authors contributed equally

29 corresponding author: Eva Candal (eva.candal@usc.es)

30 Abstract

33 The retina, whose basic cellular structure is highly conserved across vertebrates, constitutes
34 an accessible system for studying the central nervous system. In recent years, single-cell RNA-
35 sequencing studies have uncovered cellular diversity in the retina of a variety of species,
36 providing new insights on retinal evolution and development. However, similar data in
37 cartilaginous fishes, the sister group to all other extant jawed vertebrates, are still lacking.
38 Here, we present a single-nucleus RNA-sequencing atlas of the postnatal retina of the catshark
39 *Scyliorhinus canicula*, consisting of the expression profiles for 17,438 individual cells from
40 three female, juvenile catshark specimens. Unsupervised clustering revealed 22 distinct cell
41 types comprising all major retinal cell classes, as well as retinal progenitor cells (whose
42 presence reflects the persistence of proliferative activity in postnatal stages in sharks) and
43 oligodendrocytes. Thus, our dataset serves as a foundation for further studies on the
44 development and function of the catshark retina. Moreover, integration of our atlas with data
45 from other species will allow for a better understanding of vertebrate retinal evolution.

47 **Background & Summary**

48

49 The neural retina shows a remarkable degree of conservation in its cellular structure in all
50 extant vertebrates^{1–3}. This basic plan consists of five neuronal cell classes and one glial cell
51 class, whose somata are arrayed in three nuclear layers, interspersed with two plexiform
52 layers, where synapses occur (**Fig. 1a**). The outer nuclear layer (ONL) contains photoreceptors
53 (PRs), the light-sensitive cells of the retina, which can usually be classified in two
54 morphologically and functionally distinct major types, cones and rods, responsible for
55 photopic and scotopic vision, respectively. In turn, the inner nuclear layer (INL) hosts three
56 types of interneurons, namely horizontal cells (HCs), bipolar cells (BCs) and amacrine cells
57 (ACs), which receive, integrate, modulate and transmit the signals coming from
58 photoreceptors to retinal ganglion cells (RGCs). RGCs are located in the ganglion cell layer
59 (GCL) and project their axons through the optic nerve to the visual processing centres of the
60 brain. Besides, the retina contains a major glial cell class, Müller glia (MG), a type of radial glial
61 cells whose nuclei are located within the INL. Other glial cell types, such as oligodendrocytes,
62 microglia or astrocytes, may be present in the innermost layers of the retina, but, unlike MG,
63 these are not derived from the optic cup; instead, they originate in other parts of the brain
64 and migrate into the eye through the optic nerve⁴.

65 Most of these cell classes can be subdivided into a number of cell types with diverse
66 morphological, functional and molecular properties^{5–7}. In recent years, high-throughput
67 single-cell RNA sequencing (scRNA-seq) studies have provided unprecedented insights into
68 molecular cell type diversity in the mature and developing vertebrate retina^{6,8–10}. Although
69 most studies have focused on the retina of mammals^{11–32} (particularly that of rodents^{12–18} and
70 primates^{19–32}), cellular atlases of the chick^{13,33}, brown anole lizard¹¹, zebrafish^{9,13,34–40} and sea
71 lamprey^{11,41} retinas have also been generated to date, providing new resources to study the
72 evolution and development of vertebrate retinal cell types. However, scRNA-seq studies on
73 the retina of cartilaginous fishes are still lacking.

74 Given their phylogenetic position as the sister group to all other extant gnathostomes (**Fig.**
75 **1b**), chondrichthyans (sharks, rays and chimaeras) constitute a particularly interesting group
76 to study retinal evolution^{42–44}. Among cartilaginous fishes, the shark *Scyliorhinus canicula*
77 (Linnaeus, 1758), also known as the small-spotted catshark or the lesser-spotted dogfish,
78 stands as a suitable model for experimental studies, owing to its abundance, relatively small
79 size and accessible oviparous development⁴³. Furthermore, the catshark retina shows
80 persistent cell proliferation in postnatal stages^{45,46} (similar to other fishes⁴⁷), making *S. canicula*
81 an interesting species for the study of postnatal retinal neurogenesis.

82 In this study, we generated a single-nucleus RNA-sequencing (snRNA-seq) atlas of the
83 postnatal retina of *S. canicula* (**Fig. 1c**). Early juvenile specimens were chosen to allow profiling
84 of both mature and progenitor cell types, since previous work has shown that cell proliferation
85 decreases as the animal grows, with mitotic activity being virtually absent in sexually mature
86 adults^{45,48}. Thus, we used three retinas from three female juvenile catsharks to generate a
87 dataset consisting of 17,438 high quality nuclei. Unsupervised clustering revealed 22 cell types
88 representing all major retinal cell classes, as well as retinal progenitor cells and
89 oligodendrocytes. This constitutes, to the best of our knowledge, the first single-cell
90 transcriptomic study of the retina of a chondrichthyan, providing a groundwork for
91 comparative studies on the evolution of both retinal cell type diversity and retinal
92 neurogenesis.

93

94 **Methods**

95

96 **Animals**

97 Three female, juvenile specimens of *S. canicula*, with a total length of 10.5 to 11.1 cm (**Table**
98 **1**) were kindly provided by the Aquarium Finisterrae in A Coruña (Spain) and kept in artificial

99 seawater tanks under standard conditions of temperature (15-16 °C), pH (7.5-8.5) and salinity
100 (35 g/L). All procedures were performed in accordance with the guidelines for animal
101 experimentation established by the European Union and the Spanish government and were
102 approved by the Bioethics Committee of the University of Santiago de Compostela (license
103 number 15004/2022/001).

104

105 **Retina sampling**

106 Animals were deeply anaesthetised with 0.5% tricaine methanesulfonate (MS-222; Thermo
107 Fisher Scientific, 118000500) in seawater. The animals were removed from water, the eyes
108 enucleated, and the retinas (one from each specimen, n = 3) were dissected out under a
109 stereomicroscope. Retinas were immediately put in Eppendorf tubes and frozen in liquid
110 nitrogen. Retinal samples were kept at -80 °C until they were further processed for nuclei
111 isolation and RNA sequencing.

112

113 **Nuclei isolation and snRNA-seq data generation**

114 Retina nuclei were extracted following a published protocol⁴⁹ with small modifications. The
115 frozen retinas were homogenised using a micropesle in 400 µL ice-cold homogenisation
116 buffer (250 mM sucrose, 25 mM KCl, 5 mM MgCl₂, 10 mM Tris-HCl [pH 8], 0.1% IGEPAL, 1 µM
117 dithiothreitol [DTT], 0.4 U/µL Murine RNase Inhibitor [New England BioLabs, M0314L], and 0.2
118 U/µL SUPERase-In [Ambion, AM2694]). The homogenates were triturated gently using a p1000
119 tip for 10 times, incubated on ice for 5 min and then centrifuged at 100 g for 1 min at 4 °C to
120 pellet any unlysed tissue chunks. The supernatant was transferred into another 1.5 mL
121 Eppendorf tube and centrifuged at 400 g for 4 min at 4 °C to collect nuclei. The nuclei were
122 washed twice in 400 µL homogenisation buffer and strained using a 40 µm Flowmi strainer
123 (Sigma, BAH136800040) during the second wash step to remove nuclei aggregates. The final
124 nuclei pellet was resuspended in 30-50 µL Nuclei Buffer (10x Genomics, PN-2000207). To
125 estimate the nuclei concentration, nuclei aliquots were diluted in phosphate-buffered-saline
126 (PBS) with Hoechst and propidium iodide (PI) DNA dyes and counted on Countless II FL
127 Automated Cell Counter (Thermo Fisher Scientific, RRID: SCR_020236). Around 15,000 nuclei
128 were used as input for the snRNA-seq experiment. The Chromium Next GEM Single Cell 3'
129 Reagent Kits v3.1 (PN-1000121, PN-1000120, and PN-1000213) were used to make snRNA-seq
130 libraries. Libraries were quantified on a Qubit Fluorometer (Thermo Fisher Scientific; RRID:
131 SCR_018095) and quality checked on a Fragment Analyzer (Agilent; RRID: SCR_019417).
132 Libraries were sequenced on NextSeq550 (Illumina; RRID: SCR_016381; 28 cycles for Read 1,
133 56 cycles for Read 2, 8 cycles for i7 index).

134

135 **Genome indexing and read alignment**

136 Genome indexing and library mapping was performed with STAR (v2.7.10a)⁵⁰. The *S. canicula*
137 genome assembly sScyCan 1.1⁵¹ (GCF_902713615.1;
138 GCF_902713615.1_sScyCan1.1_genomic.fna) and its associated annotation in GFF format
139 (GCF_902713615.1_sScyCan1.1_genomic.gff) were downloaded from the National Center for
140 Biotechnology Information (NCBI). The mitochondria (NC_001950.1) annotations within the
141 GFF file were manually edited to convert “CDS” annotations to “exon” annotations and to
142 convert all annotations of “tRNA” and “rRNA” to “gene” annotation. This was done to ensure
143 mitochondrial gene annotations were consistent with those of the nuclear genes as STAR
144 assigns transcripts to “exon” annotations in the .gff file. The GFF annotation file was converted
145 to GTF format using gffread (v0.10.1)⁵². The genome and its annotation (GTF) were indexed
146 using STAR (--runMode genomeGenerate). Each library was then mapped against the genome
147 with the 10x V3 cell barcode whitelist (3M-february-2018.txt) and using standard parameters
148 for single cell libraries (--soloMultiMappers Unique --soloBarcodeReadLength 28 --soloType
149 CB_UML_Simple --soloUMllen 12 -- soloCBwhitelist 3M-february-2018.txt --soloFeatures
150 GeneFull --clipAdapterType CellRanger4 --outFilterScoreMin 20 --soloCBmatchWLtype

151 1MM_multi_Nbase_pseudocounts --soloUMIfiltering MultiGeneUMI_CR --soloUMIdedup
152 1MM_CR --readFilesCommand zcat --outSAMtype BAM Unsorted). The raw (unfiltered) files
153 (*genes.tsv*, *barcodes.tsv*, and *matrix mtx*) generated for each sample were then used for
154 downstream analysis. On average, there were 274 million reads per sample with 94% of reads
155 with valid barcodes, and a 45% saturation. A summary of the STAR output statistics for each
156 sample can be found in **Table 2**.

157

158 **Bioinformatic quality control**

159 Samples were then analysed in an R (v4) environment using Seurat (v4.3.0)⁵³. We created
160 Seurat objects for each library after removing nuclei with less than 200 features and features
161 occurring in fewer than three nuclei. Nuclei where mitochondrial (mtDNA) features accounted
162 for 10% or more of their total unique molecular identifiers (UMIs) were removed before
163 removing all mtDNA features. After sub-setting the Seurat object into individual samples,
164 upper and lower thresholds for UMI and feature counts per nuclei were then applied
165 individually to each sample based on knee plot visualisation. In sample 1, nuclei with more
166 than 1,000 but less than 20,000 UMIs and more than 500 but less than 5,500 features were
167 retained. In sample 2, nuclei with more than 500 but less than 24,000 UMIs and more than
168 500 but less than 6,500 features were retained. Finally, in sample 3, nuclei with more than 750
169 but less than 20,000 UMIs and more than 300 but less than 7,000 features were retained.

170 Samples were then merged into a single Seurat object before splitting samples again into
171 individual sample datasets. This was done to ensure that the same features were considered
172 across samples. Counts were then normalised for each sample using the “NormalizeData”
173 function prior to calculating cell cycle scores using the “CellCycleScoring” function (see
174 **Supplementary Table 1** for list of genes used). The “v2” SCTransform version with the
175 glmGamPoi method (v1.9.0)⁵⁴ was used to normalise RNA counts for each sample, regressing
176 out scores for the S and G2M cell cycle stages. Linear dimension reduction was conducted for
177 each sample using the “RunPCA” function with 50 PCs. After consulting Elbowplots for each
178 sample, a Uniform Manifold Approximation and Projection (UMAP) using 20 principal
179 components (PCs) was run for each sample and the “FindNeighbours” function was applied
180 using 20 PCs, before using the “FindClusters” function with a resolution of 0.5. DoubletFinder
181 (v2.0.3)⁵⁵ was then applied independently to each sample selecting pK values with the highest
182 associated mean-variance normalised bimodality coefficient (BCmvn) value. We assumed a 4%
183 doublet formation rate (based on the Chromium instrument specifications) and adjusted for
184 homotypic doublets.

185

186 **Clustering and differential gene expression analyses**

187 Samples were integrated using 2000 features and anchors that were identified with the “rpca”
188 reduction method and the “FindIntegrationAnchors” function. A principal component analysis
189 (PCA) was rerun on the integrated dataset using 50 PCs, and 30 PCs were used for subsequent
190 UMAP generation and clustering with a resolution of 0.5. Markers for each cluster were
191 assessed using the logistic regression method and the FindAllMarkers function on the “SCT”
192 assay and “data” slot, using sample ID as a latent variable to help reduce batch effects among
193 samples. We used a pseudocount of 0.001, set a p-value threshold of 0.01, and only considered
194 genes that were upregulated, expressed in at least 25% of all nuclei (in either of the compared
195 groups), and demonstrated a threshold of 0.25 X difference (log-scale) between the two
196 compared groups. Three clusters that were mostly composed of cells from a single sample and
197 did not show differential expression of typical retinal cell marker genes were removed (see
198 below; **Supplementary Table 2** shows differentially expressed genes in the removed clusters),
199 and all remaining cells were re-clustered using the same parameters. The same differential
200 expression analysis was applied to various groups of clusters (**Table 3**) to identify marker genes
201 for cell classes composed of several clusters.

202

203 **Cluster annotation**

204 To assign a cell class identity to each cluster, we elaborated a list of marker genes reported in
205 previous studies on other vertebrate species^{11–15,18–21,23,25–31,33,35,41}. Putative orthologues in the
206 *S. canicula* genome were identified by comparing the sequence of the mouse gene (genome
207 assembly GRCm39, GCF_000001635.27)⁵⁶ with the *S. canicula* genome assembly sScyCan1.1
208 (GCF_902713615.1)⁵¹ using Blastn⁵⁷. For marker genes absent from the mouse genome, either
209 the human (genome assembly GRCh38.p14, GCF_000001405.40)⁵⁸ or zebrafish (genome
210 assembly GRCz11, GCF_000002035.6)⁵⁹ genes were used. All marker gene sequences were
211 obtained from GenBank⁶⁰. Marker genes present in the *S. canicula* genome were then
212 visualised in our dataset using the “FeaturePlot” and “DotPlot” functions of Seurat. This,
213 coupled with the examination of the top differentially expressed genes in each cluster (see
214 above), allowed us to assign all clusters in the final object to known retinal cell classes (see
215 Technical Validation).

216

217 **Gene nomenclature**

218 For the sake of readability, we decided to change the symbols of genes annotated with a LOC
219 number in the main text and figures of the present article. We replaced LOC numbers for
220 symbols based on the identification of their protein products, adding an “-l” at the end for
221 those annotated as “-like”, except for uncharacterised genes, which were left with their LOC
222 number. **Supplementary Table 3** shows the correspondence between the symbols used in the
223 text and the sScyCan1.1 annotation, which is the one used in the dataset.

224 It should also be noted that many *S. canicula* genes follow the nomenclature used in zebrafish,
225 including a letter or number at the end of their symbol. Since teleosts experienced an
226 additional whole genome duplication after diverging from cartilaginous fishes⁶¹, many gene
227 paralogues present in zebrafish are absent from the catshark genome. Therefore, current gene
228 symbols do not accurately reflect the existence of paralogues in *S. canicula*, nor their
229 correspondence to specific zebrafish paralogues.

230

231 **Data Records**

232

233 Raw sequencing data for each sample (.fastq files) have been uploaded to the NCBI Sequence
234 Read Archive (SRA) under BioProject accession number PRJNA1056918⁶². For each sample,
235 STAR raw output files, i.e. expression matrices for each gene in each cell (matrix mtx),
236 barcodes (barcodes tsv) and genes (features tsv), have been uploaded to Figshare (doi: XXX).
237 The final annotated Seurat object (Scyliorhinus retina rds) is also available on Figshare.
238 Two .xlsx files containing the list of differentially expressed genes in each cluster and each cell
239 class (see **Table 3**) have been uploaded to Figshare. For each gene, the p-value (“p_val”),
240 adjusted p-value (“p_val_adj”), average log₂ fold change (“avg_log2FC”), the percentage of
241 cells expressing that gene in the present cluster (“pct.1”) and the percentage of cells
242 expressing said gene in the rest of the dataset (“pct.2”) are provided.

243

244 **Technical Validation**

245

246 **Quality control**

247 Retinas from three similarly sized, female, juvenile *Scyliorhinus canicula* specimens (**Table 1**)
248 were used to generate the snRNA-seq dataset. To ensure that all the obtained barcodes
249 correspond to viable nuclei, we established selection criteria based on feature counts, UMI
250 counts and expression of mitochondrial genes (**Fig. 2a, b**). Prior to filtering, the three samples
251 showed a similar number of nuclei (**Table 4**), features and UMIs, with the proportion of
252 mitochondrial transcripts being higher in sample 1 and lower in sample 3 (**Fig. 2a**). As
253 expected, there was a positive correlation between the number of detected genes and the
254 number of UMIs, whereas a negative correlation was observed between the expression levels

255 of mitochondrial genes and both gene counts and UMI counts, with no major differences
256 between samples (**Fig. 2c**). Quality control filtering was performed by removing nuclei with
257 mitochondrial transcripts representing more than 10% of the total counts, and upper and
258 lower thresholds for UMI and number of unique genes were defined for each sample (see
259 Methods). After filtering, initial clustering analyses revealed three clusters that were mostly
260 composed of cells from a single sample that did not show expression of typical retinal cell
261 marker genes (**Supplementary Table 2**). Since these nuclei most likely correspond to either
262 low quality cells or non-retinal cells, they were removed from the dataset. The final object was
263 composed of 17,438 cells containing 23,489 features (unique genes). There were no major
264 differences in the number of unique genes, UMI count (number of transcripts) or
265 mitochondrial feature levels between samples (**Fig. 2b, d**). However, sample 3 yielded a higher
266 number of cells (**Table 4**), which can be attributed to minor technical differences in retinal
267 dissection and/or library preparation.

268

269 Cluster annotation

270 Unsupervised clustering of filtered cells revealed 22 clusters (**Fig. 3a**), all of which were present
271 in generally similar proportions in the three samples (**Fig. 3b**), with cells from the three retinas
272 showing similar distributions across the UMAP (**Fig. 3c**), thus confirming the similarity of the
273 samples. To annotate the clusters, we analysed the expression levels of known marker genes
274 from other species (see Methods) for the major retinal cell classes or subclasses (**Fig. 4a, b**).
275 This allowed us to divide cells into the six major retinal cell classes (PRs, HCs, BCs, ACs, RGCs
276 and MG), as well as to identify two clusters of retinal progenitor cells (RPCs) and a single cluster
277 of oligodendrocytes (OLs) (**Fig. 3a**).

278 Three clusters could be identified as rod PRs by the expression of genes such as *rho*, *pdc-l* or
279 *pde6a*⁶³. Expression of established cone PR marker genes (not shown) was either present in
280 rod clusters or virtually non-existing. This is in accordance with previous observations that *S.
281 canicula* has either scarce cones⁶⁴ or a pure-rod retina^{46,65} (reviewed in Ferreiro-Galve *et al.*⁴⁶),
282 similar to some other benthic sharks^{65,66} and the skate⁶⁷. A fourth cluster that did not show
283 high levels of most rod markers but showed significant expression of *nr2e3* and *neurod1*,
284 known markers of rod precursors/progenitors⁶⁸, was thus annotated as PR precursor cells.
285 Since rod PRs usually comprise a single cell type^{33,38,69} (with some exceptions, such as those of
286 the amphibian retina⁷⁰), the four PR clusters identified here could correspond to different
287 states of PR differentiation, but further research is needed to confirm this.

288 Regarding retinal interneurons, a single cluster of HCs (expressing the canonical marker
289 *onecut3a*^{33,71}) and 3 clusters of BCs (expressing *vsx1* and *vsx2*^{11,14,72}, as well as high levels of
290 *isl1* in one of the BC clusters, confirming previous immunohistochemical results⁷³) could be
291 identified in our dataset. We also found eight clusters of ACs, most of which showed high levels
292 of *pax6*, confirming previous results⁷⁴. The AC clusters could be further divided into three
293 subclasses according to the expression of small molecule neurotransmitter-associated genes.
294 Thus, we found four clusters of GABAergic ACs expressing *gad1* and/or *gad2*^{18,75}; a single
295 cluster of cholinergic (starburst) ACs, which show high levels of *chata* (similar to those
296 described in *Squalus*⁷⁶); and three clusters of glycinergic ACs, which show high levels of glycine
297 transporters *slc6a5* and *slc6a9*¹⁸. Furthermore, two clusters of RGCs (expressing canonical
298 markers, such as *nefl-1*⁴⁵) could be recognised.

299 MG were represented by a single cluster with high levels of *rlbp1b*^{11,77} and *glul* (the gene
300 encoding glutamine synthetase, whose expression in *S. canicula* MG has previously been
301 described by means of immunohistochemistry^{73,78}). Two clusters of RPCs could also be
302 identified by the expression of cell proliferation markers (*mki67-l*^{19,79}, *pcna*^{45,46,78}) and typical
303 markers of retinal progenitors (*btg2-l*, *rx3*¹²). Finally, a small cluster of OLs was identified by
304 high levels of *olig2-l* and *mbp* expression^{13,33}, probably corresponding to cells from the optic
305 nerve head or the optic nerve fibres layer, where myelinated fibres are present in other
306 elasmobranchs⁴². A remarkable absence from our dataset are microglial cells, which are known

307 to be present in the innermost retinal layers of the postnatal retina of *S. canicula*⁸⁰. This is
308 most likely due to microglia being lost in the nuclei dissociation or quality control filtering
309 processes.

310 To further validate cluster annotation and find novel markers specific to the *S. canicula* retinal
311 cell classes, we identified marker genes (differential gene expression analyses vs the remaining
312 cells in the dataset), both for individual clusters and for clusters grouped into
313 classes/subclasses (Table 3). Fig. 4c shows the top marker genes for each class-level group,
314 including both established and novel marker genes. For a complete list, see Data Records.
315 Overall, the expression of marker genes confirms that our atlas comprises all major cell classes
316 expected in the juvenile catshark retina, although some low abundant cell types (e.g.
317 microglia) could be absent from the dataset. Thus, this dataset will provide a groundwork for
318 studies on cell type diversity in the shark retina, allowing a better understanding of vertebrate
319 retinal evolution and development.

320

321 **Usage Notes**

322

323 All the code used to analyse the dataset is available in GitHub (see Code Availability). Raw
324 .fastq files are standard Illumina sequencing files for 10x Genomics single-cell RNA sequencing
325 libraries, and as such they can be processed using any typical single-cell analysis software
326 (STAR⁵⁰, as in our work, or Cell Ranger⁸¹, Kallisto⁸², Alevin⁸³, etc.). STAR output files for each
327 sample can be loaded into Seurat using the “ReadSTARsolo” function, and then merged into a
328 single Seurat object using the “merge” function. Finally, the *Scyliorhinus_retina.rds* file is a
329 Seurat object with the processed dataset that can be loaded into R with “ReadRDS”.

330

331 **Code Availability**

332

333 The code used to process the raw sequencing files and generate all the results presented in
334 this study can be found in https://github.com/Roslin-Aquaculture/SHARK_retina.

335

336 **Acknowledgements**

337

338 This work was supported by grant ED431C 2021/18 funded by Xunta de Galicia to E.C., and
339 grant PID2020-115121GB-I00 funded by MICIU/AEI/10.13039/501100011033 to A.B.-I. N.V.-V.
340 was supported by grant FPU21/03076 funded by Ministerio de Ciencia, Innovación y
341 Universidades. D.R. was supported by the Axencia Galega the Innovación (GAIN, Xunta de
342 Galicia) as part of the Oportunus programme, and by BBSRC Institute Strategic Grants to the
343 Roslin Institute (BBS/E/20002172, BBS/E/D/30002275, BBS/E/D/10002070 and
344 BBS/E/RL/230002A). S.S. gratefully acknowledges an NSERC PDF award. This project has
345 received funding from the European Research Council (ERC) under the European Union’s
346 Horizon 2020 research and innovation programme (VerteBrain to H.K., grant agreement no.
347 101019268).

348

349 **Author contributions**

350

351 Conceptualisation: N.V.-V., I.H.-N., A.B.-I., E.C. Data acquisition: I.H.-N., P.C.-P., S.S., P.R.V.,
352 F.H.-S., X.Y., C.S., J.S., S.M. (provided early access to the catshark genome), H.K. (supervision),
353 D.R. Data analysis: N.V.-V., P.C.-P., S.S., P.R.V., F.L., D.R., E.C. Data interpretation: N.V.-V., P.C.-
354 P., A.B.I., E.C. Writing (original draft): N.V.-V., P.C.-P., S.S., D.R., A.B.-I., E.C. Writing (review and
355 editing): N.V.-V., I.H.-N., P.C.-P., S.S., P.R.V., S.M., H.K., F.A., D.R., A.B.-I., E.C. Funding
356 acquisition: H.K., D.R., A.B.-I., E.C. Project supervision: E.C.

357

358 **Competing interests**

359
360 The authors declare no competing interests.

361 **Figure Legends**

362 **Figure 1.** Background and experimental workflow. (a) Structure of the juvenile catshark retina,
363 based on microscopy images kindly provided by Dr J. Francisco-Morcillo; cell drawings based
364 on Neumayer⁶⁴. (b) Cladogram showing relationships among major extant vertebrate groups,
365 highlighting the position of chondrichthyans as the sister group to all other gnathostomes.
366 Silhouettes from PhyloPic⁸⁴. (c) Experimental workflow. Eye diagram after Collin⁴². GCL,
367 ganglion cell layer; INL, inner nuclear layer; IPL, inner plexiform layer; ONL, outer nuclear layer;
368 OPL, outer plexiform layer; OS, photoreceptor outer segments.

369
370
371 **Figure 2.** Quality control for snRNA-seq data. (a, b) Violin plots showing: left, the number of
372 detected unique genes (“nFeature_RNA”); middle, the number of unique molecular identifiers
373 (UMIs, “nCount_RNA”); and right, percentage of mitochondrial genes (“percent.mt”) in each
374 cell from each sample before (a) and after (b) quality control. Note that all mitochondrial
375 features were removed from the analyses after quality control (see Methods). (c) Scatter plots
376 showing the relationship between gene counts and UMI counts (left), UMI counts and
377 percentage of mitochondrial genes (middle), together with gene counts and percentage of
378 mitochondrial genes (right) in the three samples before quality control. (d) Gene counts (left),
379 UMI counts (middle) and percentage of mitochondrial genes (right) mapped onto the UMAP.

380
381
382 **Figure 3.** Clustering of snRNA-seq data reveals cell heterogeneity in the juvenile catshark
383 retina. (a) UMAP of retinal cells showing their unbiased assignment to the 22 clusters
384 identified in this study. For abbreviations, see **Table 3**. (b) Barplots showing the proportions of
385 each cluster for each sample. (c) Separate UMAPs of cells from each sample, coloured
386 according to their assigned identities.

387
388 **Figure 4.** Expression of marker genes used for cluster annotation. (a) Dot plot showing
389 expression levels of marker genes selected for identification of retinal cell classes (cluster
390 annotation). (b) UMAPs showing expression of selected canonical marker genes. (c) Dot plot
391 showing expression of the top three differentially expressed genes from class-level groupings
392 (see text and **Table 3** for details). See Methods and **Supplementary Table 3** for information on
393 gene nomenclature.

394

395 **Tables**
396

Sample	Total length (cm)	Sex
Sample 1	11.0	Female
Sample 2	10.5	Female
Sample 3	11.1	Female

397 **Table 1.** Sample information.
398

Sample	Sample 1	Sample 2	Sample 3
Number of reads	229,861,905	249,344,842	343,563,083
Reads with valid barcodes	0.960049	0.932741	0.917902
Sequencing saturation	0.502799	0.521001	0.338812
Q30 bases in CB + UMI	0.957978	0.95938	0.961753
Q30 bases in RNA read	0.89873	0.90096	0.888598
Reads mapped to genome: unique + multiple	0.88851	0.846251	0.647372
Reads mapped to genome: unique	0.781012	0.711432	0.518868
Reads mapped to GeneFull: unique + multiple GeneFull	0.693977	0.471452	0.354986
Reads mapped to GeneFull: unique GeneFull	0.642748	0.424422	0.314171
Estimated number of cells	3,028	1,074	2,521
Unique reads in cells mapped to GeneFull	62,372,962	34,713,678	39,214,416
Fraction of unique reads in cells	0.422171	0.328021	0.363307
Mean reads per cell	20,598	32,321	15,555
Median reads per cell	15,254	21,413	11,331
UMIs in cells	30,760,018	16,433,368	25,334,077
Mean UMIs per cell	10,158	15,301	10,049
Median UMIs per cell	7,593	10,144	7,340
Mean GeneFull per cell	3,508	4,872	3,988
Median GeneFull per cell	3,170	4,285	3,540
Total GeneFull Detected	23,271	23,076	23,449

399 **Table 2.** Summary statistics for STAR outputs for each sample. Note that raw files were used
400 for downstream analysis (which includes all barcodes, not just those estimated to be viable
401 cells by STAR). Therefore, the statistics relating to STAR-assigned cells are not necessarily
402 relevant but are provided for the reader's interest.
403

Group	Abbreviation	Clusters
Rod photoreceptors	PR_Rod	PR_Rod1, PR_Rod2, PR_Rod3
Photoreceptor precursors	PR_Precursor	PR_Precursor
Horizontal cells	HC	HC
Bipolar cells	BC	BC1, BC2, BC3
GABAergic amacrine cells	AC_GABA	AC_GABA1, AC_GABA2, AC_GABA3, AC_GABA4
Cholinergic amacrine cells	AC_ACh	AC_ACh
Glycinergic amacrine cells	AC_Gly	AC_Gly1, AC_Gly2, AC_Gly3
Retinal ganglion cells	RGC	RGC1, RGC2
Müller glia	MG	MG
Retinal progenitor cells	RPC	RPC1, RPC2
Oligodendrocytes	OL	OL

404 **Table 3.** Class/subclass-level cluster groups for differential expression analysis.

405

Sample	Sample 1	Sample 2	Sample 3	Total
Unfiltered nuclei	69,723	52,932	64,138	186,793
Filtered nuclei	4,869	4,130	8,439	17,438
Filtered features	22,472	22,458	23,014	23,489
Mean UMIs per cell	4,527	3,716	3,486	3,831
Median UMIs per cell	3,333	2,234	2,359	2,572
Mean features per cell	2,153	1,885	1,852	1,944
Median features per cell	1,892	1,434	1,502	1604
Mean percent of mitochondrial features	3.55	2.66	2.13	2.65
Median percent of mitochondrial features	3.06	2.05	1.64	2.05

406 **Table 4.** Final cell quantification and sequencing statistics. “Unfiltered nuclei” refers to the
407 number of barcodes after importing the STAR files to Seurat, excluding cells with less than 200
408 UMIs. All other parameters refer to the final object.

409

410 **Supplementary Table 1.** Genes used in cell cycle scoring.

411 **Supplementary Table 2.** Differentially expressed genes from removed clusters.

412 **Supplementary Table 3.** Gene nomenclature.

413

414 **References**

415

416 1. Baden, T. Vertebrate vision: lessons from non-model species. *Semin. Cell Dev. Biol.* **106**,
417 1–4 (2020).

418 2. Kolb, H., Nelson, R., Ahnelt, P. & Cuenca, N. Cellular organization of the vertebrate
419 retina. *Prog. Brain Res.* **131**, 3–26 (2001).

420 3. Lamb, T. D. Evolution of phototransduction, vertebrate photoreceptors and retina.
421 *Prog. Retin. Eye Res.* **36**, 52–119 (2013).

422 4. Vecino, E., Rodriguez, F. D., Ruzafa, N., Pereiro, X. & Sharma, S. C. Glia–neuron
423 interactions in the mammalian retina. *Prog. Retin. Eye Res.* **51**, 1–40 (2016).

424 5. Goetz, J. et al. Unified classification of mouse retinal ganglion cells using function,
425 morphology, and gene expression. *Cell Rep.* **40**, 111040 (2022).

426 6. Shekhar, K. & Sanes, J. R. Generating and using transcriptomically based retinal cell
427 atlases. *Annu. Rev. Vis. Sci.* **7**, 43–72 (2021).

428 7. Zeng, H. & Sanes, J. R. Neuronal cell-type classification: challenges, opportunities and
429 the path forward. *Nat. Rev. Neurosci.* **18**, 530–546 (2017).

430 8. Shiau, F., Ruzyczyk, P. A. & Clark, B. S. A single-cell guide to retinal development: cell fate
431 decisions of multipotent retinal progenitors in scRNA-seq. *Dev. Biol.* **478**, 41–58 (2021).

432 9. Vöcking, O. & Famulski, J. K. Single cell transcriptome analyses of the developing
433 zebrafish eye— perspectives and applications. *Front. Cell Dev. Biol.* **11**, 1213382 (2023).

434 10. Zhang, X., Leavey, P., Appel, H., Makrides, N. & Blackshaw, S. Molecular mechanisms
435 controlling vertebrate retinal patterning, neurogenesis, and cell fate specification.
Trends Genet. **39**, 736–757 (2023).

436 11. Hahn, J. et al. Evolution of neuronal cell classes and types in the vertebrate retina.
437 *Nature* **624**, 415–424 (2023).

438 12. Clark, B. S. et al. Single-cell RNA-seq analysis of retinal development identifies NFI
439 factors as regulating mitotic exit and late-born cell specification. *Neuron* **102**, 1111–
440 1126.e5 (2019).

441 13. Hoang, T. et al. Gene regulatory networks controlling vertebrate retinal regeneration.
442 *Science* **370**, eabb8598 (2020).

443 14. Macosko, E. Z. et al. Highly parallel genome-wide expression profiling of individual cells
444 using nanoliter droplets. *Cell* **161**, 1202–1214 (2015).

445 15. Rheaume, B. A. et al. Single cell transcriptome profiling of retinal ganglion cells
446 identifies cellular subtypes. *Nat. Commun.* **9**, 2759 (2018).

447 16. Shekhar, K. et al. Comprehensive classification of retinal bipolar neurons by single-cell
448 transcriptomics. *Cell* **166**, 1308–1323.e30 (2016).

449 17. Tran, N. M. et al. Single-cell profiles of retinal ganglion cells differing in resilience to
450 injury reveal neuroprotective genes. *Neuron* **104**, 1039–1055.e12 (2019).

451 18. Yan, W. et al. Mouse retinal cell atlas: molecular identification of over sixty amacrine
452 cell types. *J. Neurosci.* **40**, 5177–5195 (2020).

453 19. Cowan, C. S. et al. Cell types of the human retina and its organoids at single-cell
454 resolution. *Cell* **182**, 1623–1640.e34 (2020).

455 20. Gautam, P. et al. Multi-species single-cell transcriptomic analysis of ocular
456 compartment regulons. *Nat. Commun.* **12**, 5675 (2021).

457 21. Hu, F. et al. Single-cell RNA-seq reveals the cellular diversity and developmental
458 characteristics of the retinas of an infant and a young child. *Front. Cell Dev. Biol.* **10**,
459 803466 (2022).

460 22. Hu, Y. et al. Dissecting the transcriptome landscape of the human fetal neural retina
461 and retinal pigment epithelium by single-cell RNA-seq analysis. *PLoS Biol.* **17**, e3000365
462 (2019).

463 23. Liang, Q. et al. Single-nuclei RNA-seq on human retinal tissue provides improved
464 transcriptome profiling. *Nat. Commun.* **10**, 5743 (2019).

465

466 24. Lu, Y. *et al.* Single-cell analysis of human retina identifies evolutionarily conserved and
467 species-specific mechanisms controlling development. *Dev. Cell* **53**, 473-491.e9 (2020).

468 25. Lukowski, S. W. *et al.* A single-cell transcriptome atlas of the adult human retina. *EMBO J.* **38**, e100811 (2019).

470 26. Lyu, Y. *et al.* Implication of specific retinal cell-type involvement and gene expression
471 changes in AMD progression using integrative analysis of single-cell and bulk RNA-seq
472 profiling. *Sci. Rep.* **11**, 15612 (2021).

473 27. Menon, M. *et al.* Single-cell transcriptomic atlas of the human retina identifies cell
474 types associated with age-related macular degeneration. *Nat. Commun.* **10**, 4902
475 (2019).

476 28. Orozco, L. D. *et al.* Integration of eQTL and a single-cell atlas in the human eye identifies
477 causal genes for age-related macular degeneration. *Cell Rep.* **30**, 1246-1259.e6 (2020).

478 29. Peng, Y.-R. *et al.* Molecular classification and comparative taxonomies of foveal and
479 peripheral cells in primate retina. *Cell* **176**, 1222-1237.e22 (2019).

480 30. Voigt, A. P. *et al.* Molecular characterization of foveal versus peripheral human retina
481 by single-cell RNA sequencing. *Exp. Eye Res.* **184**, 234–242 (2019).

482 31. Yan, W. *et al.* Cell atlas of the human fovea and peripheral retina. *Sci. Rep.* **10**, 9802
483 (2020).

484 32. Zhang, L. *et al.* Evolutionary and developmental specialization of foveal cell types in the
485 marmoset. Preprint at <https://biorxiv.org/content/10.1101/2023.12.10.570996v1>
486 (2023).

487 33. Yamagata, M., Yan, W. & Sanes, J. R. A cell atlas of the chick retina based on single-cell
488 transcriptomics. *eLife* **10**, e63907 (2021).

489 34. Celotto, L. *et al.* Single cell RNA sequencing unravels the transcriptional network
490 underlying zebrafish retina regeneration. *eLife* **12**, RP86507 (2023).

491 35. Emmerich, K. *et al.* Molecular regulation of retinal regeneration is context specific.
492 Preprint at <https://biorxiv.org/content/10.1101/2023.11.20.567904v1> (2023).

493 36. Kölsch, Y. *et al.* Molecular classification of zebrafish retinal ganglion cells links genes to
494 cell types to behavior. *Neuron* **109**, 645-662.e9 (2021).

495 37. Lyu, P. *et al.* Common and divergent gene regulatory networks control injury-induced
496 and developmental neurogenesis in zebrafish retina. *Nat. Commun.* **14**, 8477 (2023).

497 38. Ogawa, Y. & Corbo, J. C. Partitioning of gene expression among zebrafish photoreceptor
498 subtypes. *Sci. Rep.* **11**, 17340 (2021).

499 39. Santhanam, A., Shihabeddin, E., Wei, H., Wu, J. & O'Brien, J. Molecular basis of retinal
500 remodeling in a zebrafish model of retinitis pigmentosa. *Cell. Mol. Life Sci.* **80**, 362
501 (2023).

502 40. Xu, B. *et al.* Unifying developmental programs for embryonic and post-embryonic
503 neurogenesis in the zebrafish retina. *Development* **147**, dev185660 (2020).

504 41. Wang, J. *et al.* Molecular characterization of the sea lamprey retina illuminates the
505 evolutionary origin of retinal cell types. Preprint at
506 <https://biorxiv.org/content/10.1101/2023.12.10.571000v1> (2023).

507 42. Collin, S. P. Scene through the eyes of an apex predator: a comparative analysis of the
508 shark visual system. *Clin. Exp. Optom.* **101**, 624–640 (2018).

509 43. Coolen, M. *et al.* The dogfish *Scyliorhinus canicula*: a reference in jawed vertebrates.
510 *Cold Spring Harb. Protoc.* **3**, pdb.em0111 (2008).

511 44. Hart, N. S. Vision in sharks and rays: opsin diversity and colour vision. *Semin. Cell Dev.*
512 *Biol.* **106**, 12–19 (2020).

513 45. Hernández-Núñez, I. *et al.* Loss of active neurogenesis in the adult shark retina. *Front.*
514 *Cell Dev. Biol.* **9**, 628721 (2021).

515 46. Ferreiro-Galve, S., Rodríguez-Moldes, I., Anadón, R. & Candal, E. Patterns of cell
516 proliferation and rod photoreceptor differentiation in shark retinas. *J. Chem.*
517 *Neuroanat.* **39**, 1–14 (2010).

518 47. Stenkamp, D. L. Neurogenesis in the fish retina. *Int. Rev. Cytol.* **259**, 173–224 (2007).

519 48. Rodríguez-Arrizabalaga, M., Hernández-Núñez, I., Candal, E. & Barreiro-Iglesias, A. Use
520 of vivo-morpholinos for gene knockdown in the postnatal shark retina. *Exp. Eye Res.*
521 **226**, 109333 (2023).

522 49. Krishnaswami, S. R. *et al.* Using single nuclei for RNA-seq to capture the transcriptome
523 of postmortem neurons. *Nat. Protoc.* **11**, 499–524 (2016).

524 50. Dobin, A. *et al.* STAR: ultrafast universal RNA-seq aligner. *Bioinformatics* **29**, 15–21
525 (2013).

526 51. Genome assembly sScyCan1.1. *NCBI Genome assembly database*
527 https://identifiers.org/refseq.gcf:GCF_902713615.1 (2020).

528 52. Pertea, G. & Pertea, M. GFF Utilities: GffRead and GffCompare. *F1000Res.* **9**, 304
529 (2020).

530 53. Hao, Y. *et al.* Integrated analysis of multimodal single-cell data. *Cell* **184**, 3573–3587.e29
531 (2021).

532 54. Ahlmann-Eltze, C. & Huber, W. glmGamPoi: fitting Gamma-Poisson generalized linear
533 models on single cell count data. *Bioinformatics* **36**, 5701–5702 (2021).

534 55. McGinnis, C. S., Murrow, L. M. & Gartner, Z. J. DoubletFinder: doublet detection in
535 single-cell RNA sequencing data using artificial nearest neighbors. *Cell Syst.* **8**, 329–
536 337.e4 (2019).

537 56. Genome assembly GRCh39. *NCBI Genome assembly database*
538 https://identifiers.org/refseq.gcf:GCF_000001635.27 (2020).

539 57. Camacho, C. *et al.* BLAST+: architecture and applications. *BMC Bioinformatics* **10**, 421
540 (2009).

541 58. Genome assembly GRCh38.p14. *NCBI Genome assembly database*
542 https://identifiers.org/refseq.gcf:GCF_000001405.40 (2022).

543 59. Genome assembly GRCz11. *NCBI Genome assembly database*
544 https://identifiers.org/refseq.gcf:GCF_000002035.6 (2017).

545 60. Benson, D. A. *et al.* GenBank. *Nucleic Acids Res.* **41**, D36–D42 (2012).

546 61. Glasauer, S. M. K. & Neuhauss, S. C. F. Whole-genome duplication in teleost fishes and
547 its evolutionary consequences. *Mol. Genet. Genomics* **289**, 1045–1060 (2014).

548 62. *Scyliorhinus canicula* retina single-nuclei RNA sequencing. *NCBI Sequence Read Archive*
549 <https://identifiers.org/insdc.sra:SRP480047> (2023).

550 63. Lamb, T. D. Evolution of the genes mediating phototransduction in rod and cone
551 photoreceptors. *Prog. Retin. Eye Res.* **76**, 100823 (2020).

552 64. Neumayer, L. Der feinere Bau der Selachier-Retina. *Arch. Mikr. Anat.* **48**, 83–111 (1896).

553 65. Bozzano, A., Murgia, R., Vallerga, S., Hirano J & Archer, S. The photoreceptor system in
554 the retinae of two dogfishes, *Scyliorhinus canicula* and *Galeus melastomus*: possible
555 relationship with depth distribution and predatory lifestyle. *J. Fish Biol.* **59**, 1258–1278
556 (2001).

557 66. Schieber, N. L., Collin, S. P. & Hart, N. S. Comparative retinal anatomy in four species of
558 elasmobranch. *J. Morphol.* **273**, 423–440 (2012).

559 67. Dowling, J. E. & Ripps, H. On the duplex nature of the skate retina. *J. Exp. Zool.* **256**, 55–
560 65 (1990).

561 68. Nelson, S. M., Frey, R. A., Wardwell, S. L. & Stenkamp, D. L. The developmental
562 sequence of gene expression within the rod photoreceptor lineage in embryonic
563 zebrafish. *Dev. Dyn.* **237**, 2903–2917 (2008).

564 69. Baden, T. & Osorio, D. The retinal basis of vertebrate color vision. *Annu. Rev. Vis. Sci.* **5**,
565 177–200 (2019).

566 70. Yovanovich, C. A. M. *et al.* The dual rod system of amphibians supports colour
567 discrimination at the absolute visual threshold. *Philos. Trans. R. Soc. B-Biol. Sci.* **372**,
568 20160066 (2017).

569 71. Kreplova, M. *et al.* Dose-dependent regulation of horizontal cell fate by Onecut family
570 of transcription factors. *PLoS One* **15**, e0237403 (2020).

571 72. Passini, M. A., Levine, E. M., Canger, A. K., Raymond, P. A. & Schechter, N. Vsx-1 and
572 Vsx-2: differential expression of two Paired-like homeobox genes during zebrafish and
573 goldfish retinogenesis. *J. Comp. Neurol.* **388**, 495–505 (1997).

574 73. Bejarano-Escobar, R. *et al.* Retinal histogenesis and cell differentiation in an
575 elasmobranch species, the small-spotted catshark *Scyliorhinus canicula*. *J. Anat.* **220**,
576 318–335 (2012).

577 74. Ferreiro-Galve, S., Rodríguez-Moldes, I. & Candal, E. Pax6 expression during
578 retinogenesis in sharks: comparison with markers of cell proliferation and neuronal
579 differentiation. *J. Exp. Zool. B Mol. Dev. Evol.* **318**, 91–108 (2012).

580 75. Ferreiro-Galve, S., Candal, E., Carrera, I., Anadón, R. & Rodríguez-Moldes, I. Early
581 development of GABAergic cells of the retina in sharks: an immunohistochemical study
582 with GABA and GAD antibodies. *J. Chem. Neuroanat.* **36**, 6–16 (2008).

583 76. Brandon, C. Cholinergic amacrine neurons of the dogfish retina. *Vis. Neurosci.* **6**, 553–
584 562 (1991).

585 77. Saari, J. C. & Crabb, J. W. Focus on molecules: cellular retinaldehyde-binding protein
586 (CRALBP). *Exp. Eye Res.* **81**, 245–246 (2005).

587 78. Sánchez-Farías, N. & Candal, E. Identification of radial glia progenitors in the developing
588 and adult retina of sharks. *Front. Neuroanat.* **10**, 65 (2016).

589 79. Kee, N., Sivalingam, S., Boonstra, R. & Wojtowicz, J. M. The utility of Ki-67 and BrdU as
590 proliferative markers of adult neurogenesis. *J. Neurosci. Methods* **115**, 97–105 (2002).

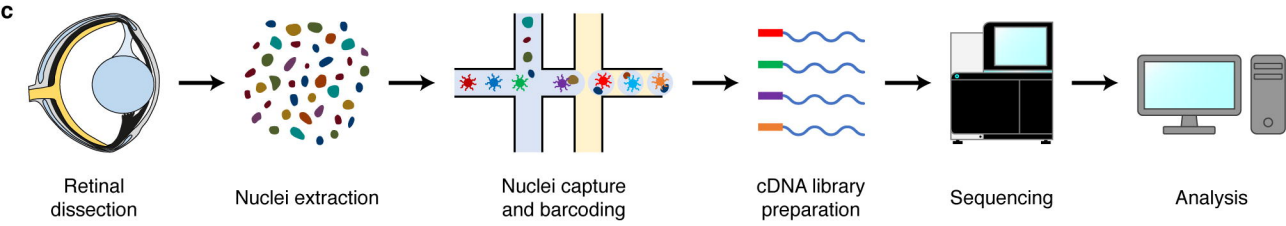
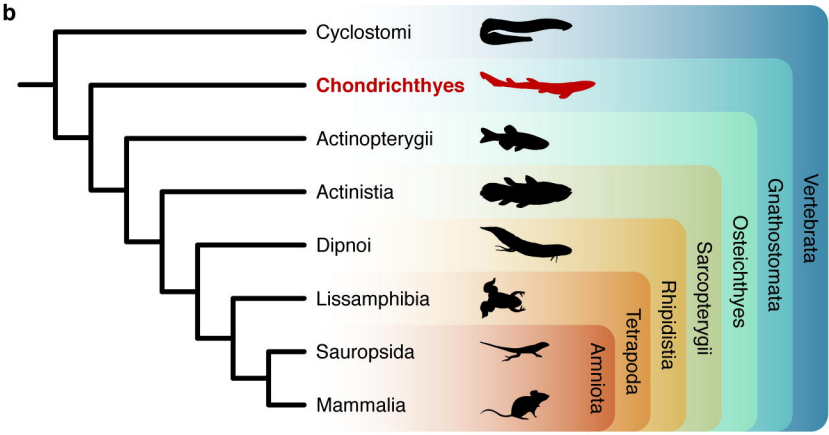
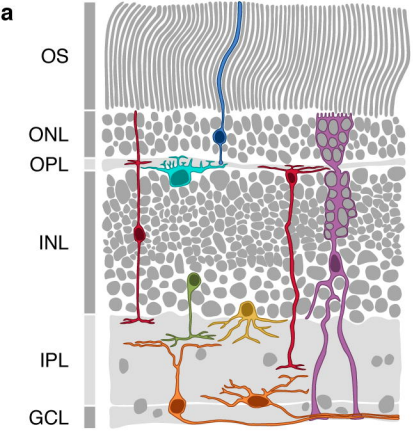
591 80. Bejarano-Escobar, R., Blasco, M., Durán, A. C., Martín-Partido, G. & Francisco-Morcillo,
592 J. Chronotopographical distribution patterns of cell death and of lectin-positive
593 macrophages/microglial cells during the visual system ontogeny of the small-spotted
594 catshark *Scyliorhinus canicula*. *J. Anat.* **223**, 171–184 (2013).

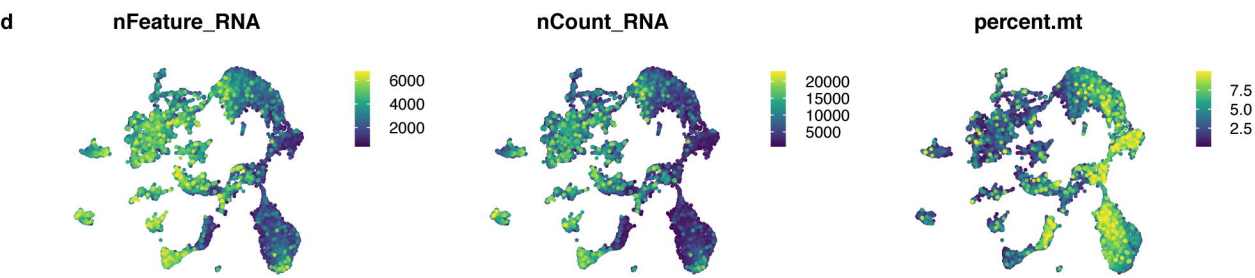
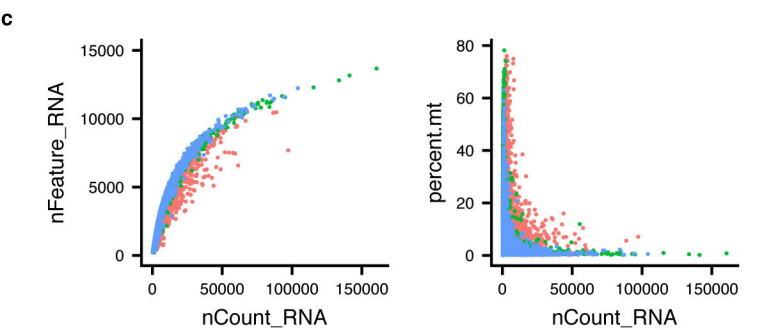
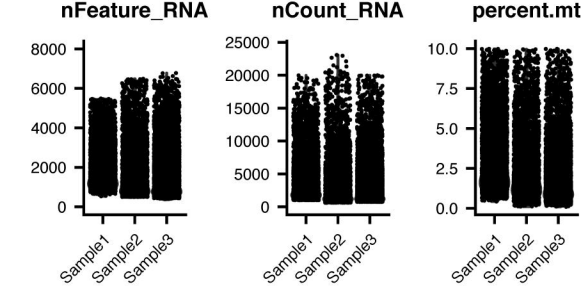
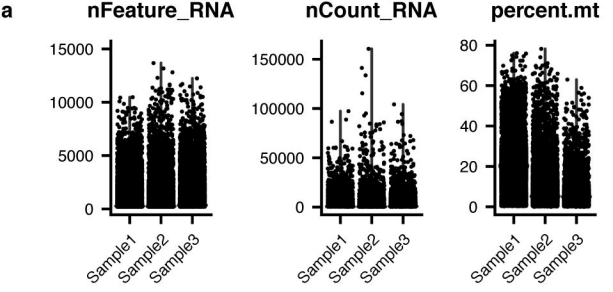
595 81. Zheng, G. X. Y. *et al.* Massively parallel digital transcriptional profiling of single cells.
596 *Nat. Commun.* **8**, 14049 (2017).

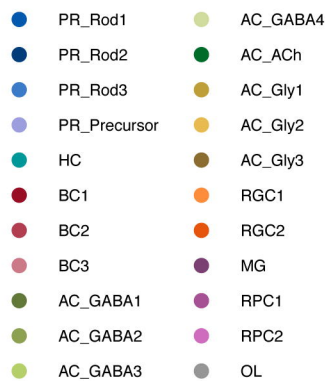
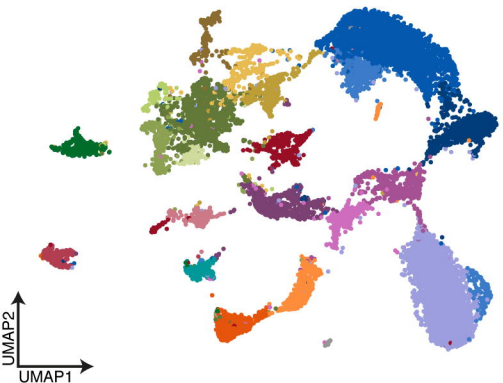
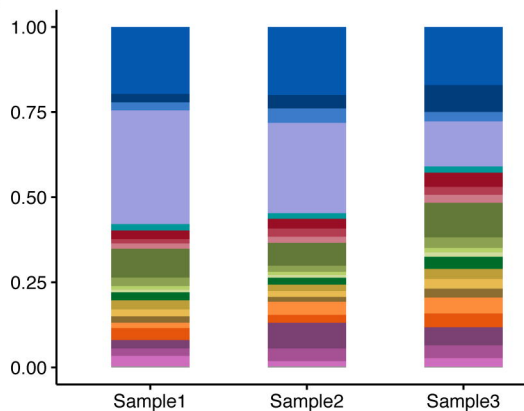
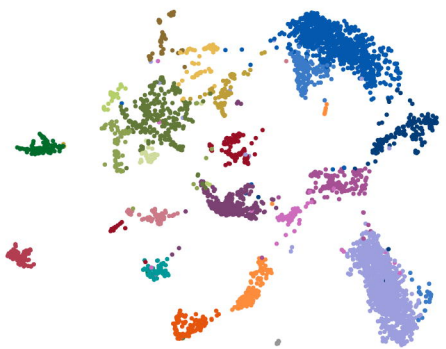
597 82. Bray, N. L., Pimentel, H., Melsted, P. & Pachter, L. Near-optimal probabilistic RNA-seq
598 quantification. *Nat. Biotechnol.* **34**, 525–527 (2016).

599 83. Srivastava, A., Malik, L., Smith, T., Sudbery, I. & Patro, R. Alevin efficiently estimates
600 accurate gene abundances from dscRNA-seq data. *Genome Biol.* **20**, 65 (2019).

601 84. Keesey, M. T. *PhyloPic* <https://www.phylopic.org/> (2024).





a**b****c****Sample1****Sample2****Sample3**